NONLINEAR FILTERING FOR EXTRACTING ORIENTATION AND TRACING TUBULAR STRUCTURES IN 2-D MEDICAL IMAGES

H. Ertan Çetingül, René Vidal, Gernot Plank and Natalia Trayanova

Department of Biomedical Engineering, Johns Hopkins University, Baltimore MD 21218, USA
{*ertan,rvidal,gernot.plank,ntrayanova*}@*jhu.edu*

ABSTRACT

We consider the problems of extracting local fiber orientation and tracing tubular structures in 2-D medical images. We first present a nonlinear filter for detecting overlaid orientations at each pixel. The filter is used to build two profiles, the *directional profile* and the *appearance profile*, which are designed to give high responses along an oriented structure. The local orientation at a pixel is then obtained from the local maxima of the product of these two profiles. We also develop an algorithm for tracing tubular structures. Starting from a user-specified seed point on the fiber, we find the next point on the fiber by locating the maxima of the *tracing profile*, which favors the smoothness of the curve as well as its alignment with the estimated orientation. We evaluate the proposed method on different medical structures such as cardiac myofibers, vessels, and microtubules.

Index Terms— Nonlinear filtering, local orientation analysis, tracing of tubular structures.

1. INTRODUCTION

Extracting local orientation and tracing tubular structures in medical images are important quantitative tools for developing precise physiological models of organs. For instance, the configuration of the myocardial fibers is crucial for modeling the electromechanical properties of the heart and understanding structural changes with myocardial infarction [1]. Likewise, the mechanical properties of cells are related to the spatial orientation of the cytoskeletal filaments. Moreover, the detection and enhancement of human vasculature can significantly improve the visualization of interventional procedures [2].

The problems of extracting local fiber orientation and tracing fibers in medical images are closely related to a primal problem in image processing: *edge detection*. This has motivated several efforts in the image processing and computer vision communities to introduce fast and robust edge detection algorithms. Most of the existing methods are based on i) the image gradient [3], ii) the image Hessian [2, 4], or iii) the structure tensor [5, 6]. In particular, Karlon et al. present a geometric algorithm based on the gradient image to extract the alignment of cytoskeletal filaments [3]. Different functions of the eigenvalues of the image Hessian are examined for vascular enhancement [2], and detection of different tubular structures [4]. Also, [7] proposes a path seeking strategy that uses both the image Hessian and image gradient to trace microtubules.

Despite the success of Hessian-based solutions in detecting tubular structures, such methods suffer from sensitivity to noise and scale, as well as non-robustness to bifurcations and crossings. Nonlinear filters can be designed to overcome these problems. For

_____

instance, in [8], multiscale elongated filters are presented for fiber detection and enhancement, whereas [9] uses the characteristics of the local intensity profile for detecting vessels.

In this paper, we propose a robust nonlinear filter that avoids the computation of image derivatives. We extract overlaid orientations at a pixel from the values of two different profiles. The first profile, called the *directional profile*, is built by comparing the intensity variations along the oriented structure to those across the structure. The second profile, called the *appearance profile*, is formed by examining the intensity coherence along the structure. The product of these profiles gives the probability of having an oriented structure along a given direction at each pixel. We also develop a method initiated at user-specified seeds for tracing fibers through branching points. In particular, given a point on the structure of interest, the algorithm locates the next point by finding the mode of the *tracing profile*, which favors the smoothness of the structure as well as its alignment with the aforementioned profiles. We localize the modes of the profiles, i.e., orientations to be followed, using Gaussian mixture models.

This paper is organized as follows: §2 shows the construction of the nonlinear filters; §3 presents the computation of the filter profiles; §4 describes the extraction of the local orientation along with the tracing algorithm; and §5 shows the experimental results. §6 presents the conclusions as well as directions for future research.

2. CONSTRUCTION OF THE NONLINEAR FILTERS

The proposed nonlinear filter is inspired from the design introduced in [10], which we will refer to as the *rigid filter*. This filter computes a nonlinear function of the image intensities on a neighborhood of a point of interest, which is designed to give a high response when the filter is aligned with the oriented structure. More specifically, the filter is centered at the point of interest $\boldsymbol{x} = (x_1, x_2)$, and is oriented at an angle $\theta \in (-\pi/2, \pi/2]$ with respect to the x-axis, as depicted in Fig. 1(a). The support is defined in terms of the width w and the radius r of the filter, and these parameters dictate the placement of the points $\{\boldsymbol{b}, \boldsymbol{b}_1, \boldsymbol{b}_2\}$ and $\{\boldsymbol{f}, \boldsymbol{f}_1, \boldsymbol{f}_2\}$, which form the backward and the forward parts, respectively. Note that $\{\boldsymbol{b}_1, \boldsymbol{b}_2\}$ and $\{\boldsymbol{f}_1, \boldsymbol{f}_2\}$ form *antipodal* pairs with respect to $\boldsymbol{b}$ and $\boldsymbol{f}$, respectively. The filter is designed to give a high response when the variation of intensity between $\boldsymbol{f}$ and $\boldsymbol{b}$ is small compared to the variations of intensity in the perpendicular direction. The filter is quite effective in detecting road-like structures, as shown in [10].

Unfortunately, the filter depicted in Fig. 1(a) can have difficulties in detecting multiple orientations at a *branching* point, because the portion $\overline{\boldsymbol{b}\boldsymbol{f}}$ is rigid. For instance, the portion $\overline{\boldsymbol{b}\boldsymbol{f}}$ will not be perfectly aligned with the branches at a Y-junction. This is a common occurrence in medical images. We thus modify the filter to give a high response at more than one orientation. The *pivoting filter*, shown in

Fig. 1(b), is a variant of the rigid filter such that its backward portion $\{\overline{\boldsymbol{b}_1\boldsymbol{b}_2}, \overline{\boldsymbol{b}\boldsymbol{x}}\}$ is fixed, whereas its forward portion $\{\overline{\boldsymbol{f}_1\boldsymbol{f}_2}, \overline{\boldsymbol{x}\boldsymbol{f}}\}$ is allowed to pivot with respect to $\boldsymbol{x}$. The relative orientation at $\boldsymbol{x}$ is defined as the angle between the forward and the backward part, i.e., $\theta := \angle(\overline{\boldsymbol{b}\boldsymbol{x}}, \overline{\boldsymbol{x}\boldsymbol{f}}) \in (-\pi/2, \pi/2]$. As we shall see, this filter is particularly useful for tracing fibers through branchings.

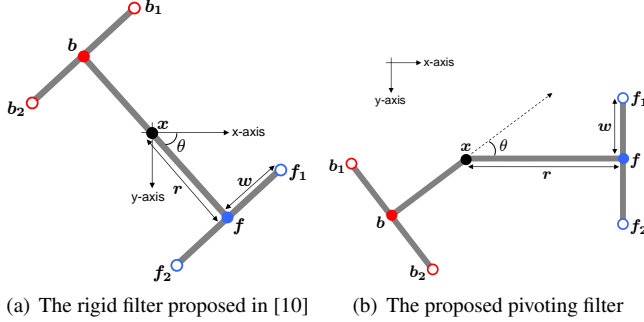(a) The rigid filter proposed in [10]   (b) The proposed pivoting filter

Fig. 1. Geometry of the nonlinear filters with key parameters

3. PROFILES FOR ORIENTATION ANALYSIS

3.1. Nonlinear Filter Response and Directional Profile

We shall now present the nonlinear response of the pivoting filter. Let $\Upsilon \subset \mathbb{R}^2$ denote the image domain. Consider a grayscale image $I : \Upsilon \to \mathbb{R}$, and denote the intensity value at a point $\boldsymbol{x} \in \Upsilon$ by $I(\boldsymbol{x})$. Also, let $\Theta \subset \mathbb{R}$ be the set of filter orientations. The response of the pivoting filter at point $\boldsymbol{x}$ along a direction $\theta \in \Theta$ is defined as[1]

$$h_{\boldsymbol{x}}(\theta) = \begin{cases} 1 & \text{if } |I(\boldsymbol{f}) - I(\boldsymbol{b})| \le \min_{i=1,2} \{|I(\boldsymbol{b}_i) - I(\boldsymbol{b})|, |I(\boldsymbol{f}_i) - I(\boldsymbol{f})|\} \\ 0 & \text{otherwise.} \end{cases} \tag{1}$$

The response of the filter in (1) can be interpreted as a voting scheme. At each pixel $\boldsymbol{x}$, the filter detects a linear structure oriented along $\theta \in \Theta$ if the absolute value of the intensity variation along the structure is less than the minimum absolute intensity variation orthogonal to the structure. However, notice that the response of the filter is 1 only when the portions $\overline{\boldsymbol{b}\boldsymbol{x}}$ and $\overline{\boldsymbol{x}\boldsymbol{f}}$ are *almost perfectly* aligned with the underlying structure of interest. A small variation of orientation will cause the filter to immediately give a 0 response.

To overcome this problem, we compute the filter response $h_{\boldsymbol{x}}(\theta)$ at several pixels in a neighborhood of $\boldsymbol{x}$ and at several orientations θ. We then aggregate and normalize these responses in order to obtain a probability distribution of the local orientation at each pixel $\boldsymbol{x}$. More specifically, let $N_{\boldsymbol{x}}$ denote a neighborhood of $\boldsymbol{x}$ of size $\omega_d \times \omega_d$. The average response of the filter on $N_{\boldsymbol{x}}$ is given by $\bar{h}_{\boldsymbol{x}}(\theta) = \sum_{\tilde{\boldsymbol{x}}_k \in N_{\boldsymbol{x}}} h_{\tilde{\boldsymbol{x}}_k}(\theta)/|N_{\boldsymbol{x}}|$, where $|N_{\boldsymbol{x}}|$ is the cardinality of $N_{\boldsymbol{x}}$. We then evaluate the average filter response on a *finite* set of orientations $\Theta = \{\theta_u\}$, where u represents the discretization index. The *directional profile*, denoted by $\mathcal{P}_{D;\boldsymbol{x}}(\theta)$, is the probability of detecting an oriented structure at point $\boldsymbol{x}$ along direction θ, i.e.,

$$\mathcal{P}_{D;\boldsymbol{x}}(\theta) = \frac{\bar{h}_{\boldsymbol{x}}(\theta)}{\sum_u \bar{h}_{\boldsymbol{x}}(\theta_u)}. \tag{2}$$

---

[1]In practice, the image is defined at discrete coordinates, i.e., $\Upsilon \subset \mathbb{Z}^2$, but the points $\{\boldsymbol{b}, \boldsymbol{b}_i, \boldsymbol{f}, \boldsymbol{f}_i\}$ may be points in $\mathbb{R}^2$ for a particular orientation θ. In such cases, we compute $I(\boldsymbol{x})$ by bilinear interpolation on a neighborhood of $\boldsymbol{x}$, $\Omega_{\boldsymbol{x}}$, i.e., $I(\boldsymbol{x}) = \sum_{\bar{\boldsymbol{x}}_k \in \Omega_{\boldsymbol{x}}} a_k I(\bar{\boldsymbol{x}}_k)$, where $\bar{\boldsymbol{x}}_k \in \mathbb{Z}^2$ and a_k are the weights of the points $\{\bar{\boldsymbol{x}}_k\}$ such that $\sum_k a_k = 1$.

3.2. Intensity Coherence and Appearance Profile

An alternative way of estimating local orientation in an image is to find image directions along which the intensity variation is small. This can be done by building a profile that measures the intensity coherence along a particular direction. In [9], Qian et al. defined a polar profile measure that reflects the probability of having a vessel at an individual point. Here, we employ a similar measure that captures the intensity coherence along $\overline{\boldsymbol{x}\boldsymbol{f}}$.

We note that the sum of the absolute intensity difference remains low if i) the pivoting portion $\overline{\boldsymbol{x}\boldsymbol{f}}$ aligns with the true fiber, and ii) the points for which the difference is computed are selected from the pivoting portion. Hence, we define the intensity coherence as

$$g_{\boldsymbol{x}}(\theta) = \frac{1}{|N_{\boldsymbol{x}}|} \sum_{\tilde{\boldsymbol{x}} \in N_{\boldsymbol{x}}} \int_0^1 |I(\tilde{\boldsymbol{x}} + \lambda(\tilde{\boldsymbol{f}} - \tilde{\boldsymbol{x}})) - I(\tilde{\boldsymbol{x}})|^2 d\lambda, \tag{3}$$

where $\tilde{\boldsymbol{f}}$ is the forward filter point calculated with respect to each $\tilde{\boldsymbol{x}} \in N_{\boldsymbol{x}}$. Note that $g_{\boldsymbol{x}}(\theta)$ is minimized when the search direction θ aligns with the true fiber orientation.

We can use the intensity coherence to define the probability of having a small appearance variation at $\boldsymbol{x}$ along θ. For this purpose, we define the *appearance profile*, denoted by $\mathcal{P}_{A;\boldsymbol{x}}(\theta)$, as

$$\mathcal{P}_{A;\boldsymbol{x}}(\theta) = Z \exp(-g_{\boldsymbol{x}}(\theta)), \tag{4}$$

where Z is a normalization constant. Notice that $\mathcal{P}_{A;\boldsymbol{x}}$ is maximized when θ aligns with the true fiber orientation. Therefore, we can use it in combination with the directional profile for orientation estimation and fiber tracing, as we will show now.

4. PROFILE-BASED ORIENTATION EXTRACTION AND FIBER TRACING

Recall that the rigid filter (Fig. 1(a)) performs well when the local structure is composed of only *one* dominant orientation or with linearly *crossing* structures, e.g., X-junctions. The pivoting filter (Fig. 1(b)), on the other hand, requires prior localization of the fixed backward portion $\{\overline{\boldsymbol{b}_1\boldsymbol{b}_2}, \overline{\boldsymbol{b}\boldsymbol{x}}\}$, and scans the region with its pivoting forward portion. Therefore, the pivoting filter is more suitable for detecting orientations at a *branching* point, hence for tracing oriented structures. We thus utilize the rigid filter for orientation extraction and the pivoting filter for fiber tracing, as described next.

4.1. Orientation Extraction

Extraction of local orientation is usually performed by analyzing the distribution of fibers at some user-specified points. The directional profile $\mathcal{P}_{D;\boldsymbol{x}}(\theta)$ and the appearance profile $\mathcal{P}_{A;\boldsymbol{x}}(\theta)$ reflect the probability of having a locally linear structure at $\boldsymbol{x}$ in the direction θ. We utilize the rigid filter to build the aforementioned profiles, and obtain the *orientation profile* $\mathcal{P}_{O;\boldsymbol{x}}(\theta)$ at $\boldsymbol{x}$ along θ as

$$\mathcal{P}_{O;\boldsymbol{x}}(\theta) = \mathcal{P}_{D;\boldsymbol{x}}(\theta) \cdot \mathcal{P}_{A;\boldsymbol{x}}(\theta). \tag{5}$$

The modes, i.e., local maxima, of the orientation profile $\mathcal{P}_{O;\boldsymbol{x}}$ give the candidate orientations at $\boldsymbol{x}$. We will describe how to find such local maxima in §4.3.

4.2. Fiber Tracing

Given two user-specified points $\boldsymbol{x}_1$ and $\boldsymbol{x}_2$, our tracing algorithm *successively* locates points $\{\boldsymbol{x}_1, \boldsymbol{x}_2, \boldsymbol{x}_3, \ldots\}$ on the fiber and represents the resulting structure as the ordered set of those points. The

tracing algorithm proceeds as follows. At each step i, we assume we are given points $\boldsymbol{x}_{i-1}$ and $\boldsymbol{x}_i$, and wish to find point $\boldsymbol{x}_{i+1}$. For this purpose, we build a pivoting filter, such as the one shown in Fig. 1(b), with $\boldsymbol{b} = \boldsymbol{x}_{i-1}$, $\boldsymbol{x} = \boldsymbol{x}_i$ and $\boldsymbol{f} = \boldsymbol{x}_{i+1}$. We want the point $\boldsymbol{x}_{i+1}$ to maximize the orientation profile, but at the same time give rise to a smooth curve. For this purpose, we define a smoothness term γ as the cosine of the angle between the segments $\overline{\boldsymbol{bx}}$ and $\overline{\boldsymbol{xf}}$, i.e.,

$$\gamma_{\boldsymbol{x}_i}(\theta) = \cos(\theta). \tag{6}$$

We then choose $\boldsymbol{x}_{i+1}$ as the point along the direction θ that maximizes the *tracing profile* at $\boldsymbol{x}_i$, $\mathcal{P}_{T;\boldsymbol{x}_i}(\theta)$, which is defined as

$$\mathcal{P}_{T;\boldsymbol{x}_i}(\theta) = \mathcal{P}_{D;\boldsymbol{x}_i}(\theta) \cdot \mathcal{P}_{A;\boldsymbol{x}_i}(\theta) \cdot \gamma_{\boldsymbol{x}_i}(\theta). \tag{7}$$

The tracing profile favors both the local smoothness of the resulting structure as well as alignment with the directional profile $\mathcal{P}_D$ and the appearance profile $\mathcal{P}_A$ at point $\boldsymbol{x}_i$ along θ. The modes of the tracing profile $\mathcal{P}_T$ give the candidate orientations at $\boldsymbol{x}_i$ to be tracked.

4.3. Mode Detection

To detect automatically the modes of the orientation profile (Eq. 5) and of the tracing profile (Eq. 7), we employ a Gaussian mixture model (GMM). The number of Gaussian components C corresponds to the maximum number of branches a fiber can divide into at a point. Thus, locating the underlying orientations at the seed point $\boldsymbol{x}$ is equivalent to computing the parameters $\{\{\mu_c\}, \{\sigma_c\}\}$ of the mixture model, which can be done using the expectation-maximization (EM) algorithm. In particular, the means of the Gaussian distributions $\{\mu_c\}$ are the candidate orientations. Notice that a GMM may overestimate the number of branches in the structure, thus an intermediate step that finds the true number of orientations is required. A simple solution is to merge any two components if the angle between their means is smaller than a user-specified threshold δ.

The means of the Gaussian distributions, after angular thresholding, represent the estimated directions at point $\boldsymbol{x}_i$. When tracing the fibers beyond $\boldsymbol{x}_i$, the next point along the c-th branch is computed as $\boldsymbol{x}_{i+1}^c = \boldsymbol{x}_i + t \cdot \mu_c$, where t is a user-specified step size. This calculation is repeated for each cluster center $\{\mu_c\}$ to track every branch starting at $\boldsymbol{x}_i$. Fig. 2 illustrates the operation of the pivoting filter at two points and shows the GMM-based extraction of local orientations on a synthetic image.
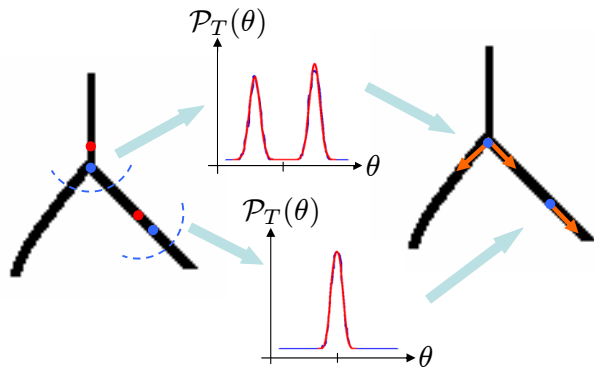

Fig. 2. Extraction of local orientation using the pivoting filter and mode detection using GMM at two analysis points $\{\boldsymbol{x}\}$ (in blue) with corresponding backward points $\{\boldsymbol{b}\}$ (in red)

5. EXPERIMENTS

5.1. Illustrative Examples

We begin by evaluating the performance of our nonlinear filter in two different types of medical data. We first extract the local orientation on microtubules assembled in vitro (Fig. 3(a)) using the rigid filter. The filter parameters are set to $\{r, w, w_d\} = \{6, 4, 5\}$. It is assumed that there is only *one dominant* orientation at each analysis point. Hence a representative vector along $\hat{\theta} = \arg\max_u \mathcal{P}_O(\theta_u)$ is placed to visualize the extracted orientations, which are also shown in Fig. 3(a). We observe that the pivoting filter successfully captures the local orientations because i) the width of all the oriented structures are approximately equal, and ii) the width w of the filter is selected such that the antipodal pairs encapsulate the fibers. We will discuss the importance of the filter geometry in §5.4.

We then trace a simple bifurcating vessel (Fig. 3(b)) using the pivoting filter. In this case, the filter parameters are set to $\{r, w, w_d, t\} = \{4, 4, 3, 2\}$, whereas the number of Gaussian components C is equal to 2, and the angular separation threshold δ between the means of the components is $\pi/3$. Fig. 3(b) also shows the result of the tracing algorithm. It is observed that the pivoting filter is able to locate the bifurcation and accurately trace the vessel.
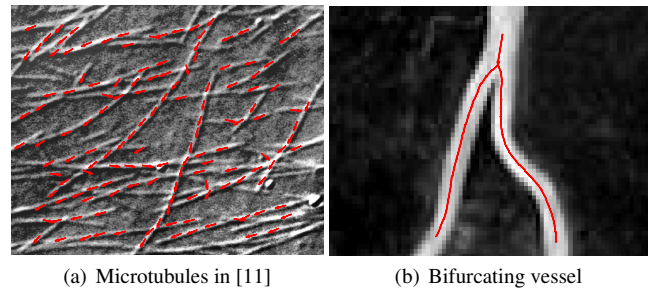

(a) Microtubules in [11]   (b) Bifurcating vessel

Fig. 3. Illustrative examples showing the performance of the filters

5.2. Tracing Microtubules

We also evaluate the performance of our tracing algorithm in microscopic microtubule images taken from [12]. The parameters of the pivoting filter are set to $\{r, w, w_d, t\} = \{4, 3, 3, 2\}$. Fig. 4 illustrates selected microtubules superimposed with their corresponding tracing results. Notice that each microtubule is independently traced and different colors are used to differentiate between crossing structures. Since the microtubules do not have any bifurcation, we set $C = 1$ and compute the mean of the tracing profile at a point $\boldsymbol{x}_i$ on a structure to find the next point $\boldsymbol{x}_{i+1}$. We observe that the algorithm yields visually correct results.
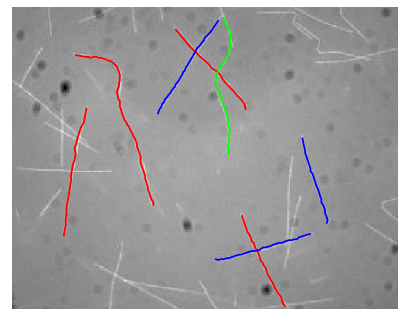

Fig. 4. Tracing of microtubules (image in [12])

5.3. Orientation Extraction on Cardiac Myofibers

The rigid filter is used to extract myofiber orientation in cardiac histology images. Figs. 5(a)-5(c) show two images with the regions of interest (ROIs) marked in blue. Fig. 5(b)-5(d) depict the extracted orientation vectors in red and the average orientation vector in blue. The filter parameters are set to $\{r, w, w_d\} = \{3, 4, 5\}$. We see that at most of the analysis points, the extracted local orientation matches that of the image fibers, and hence the average orientation vectors are visually correct. The errors are due to the small distance between individual image fibers.
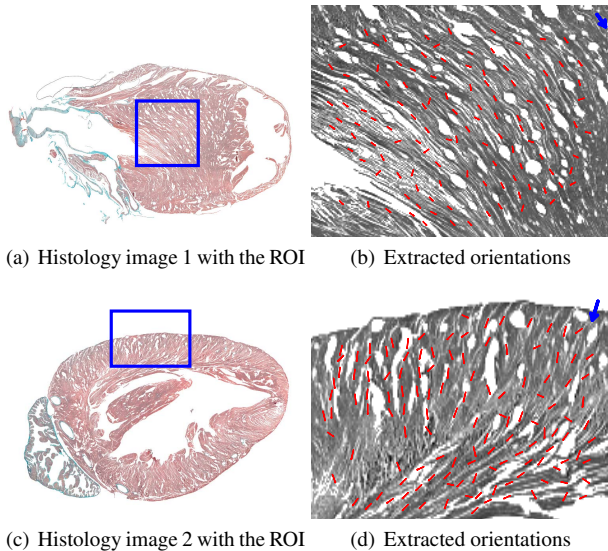

(a) Histology image 1 with the ROI (b) Extracted orientations

(c) Histology image 2 with the ROI (d) Extracted orientations

Fig. 5. Fiber orientations in cardiac histology images

We repeat the same experiment on images of the left and right ventricles of a guinea pig heart. Our results are illustrated in Fig. 6. In Fig. 6(a), the width of the myofibers and their relative position prevent us from finding an optimal size for the filter. In particular, a filter of width $w = 10$ only captures local orientations of myofibers of smaller width, but still enables us to compute the visually correct average orientation shown in blue. In Fig. 6(b), the presence of high textured areas causes erroneous orientations at some analysis points, but the average orientation vector shows the correct orientation.
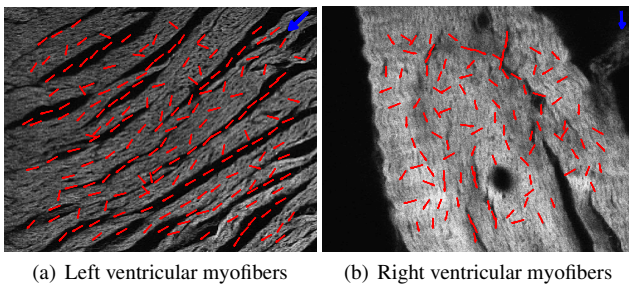

(a) Left ventricular myofibers (b) Right ventricular myofibers

Fig. 6. Orientation extraction on myofibers of a guinea pig heart

5.4. Discussions on Parameter Selection

Our experiments show that the size of the filter determines the type of structures that can correctly be detected in an image. For instance,

the distance between the antipodes, $2w$, should be larger than the width of the structure. However, the presence of nearby structures limits the value of w. Hence the minimum value of w that allows the antipodal pairs to encapsulate the fiber is the optimal value. On the other hand, the value of r becomes specially critical if the local curvature of the true fiber abruptly changes. A good strategy is to increase or decrease the value of r depending on the local curvature. The tracing step size t plays a similar role to the radius r, hence it can be adjusted as a function of the local curvature.

6. CONCLUSIONS AND FUTURE WORK

We have presented a nonlinear filtering technique to extract local spatial orientation and trace tubular structures in 2-D medical images. The rigid nonlinear filter detects the correct orientation at a point of interest, and provides the user with directional and appearance profiles, which mutually reflect the probability of observing an oriented structure as a function of direction. Likewise, our pivoting filter builds the profiles and adds a smoothness term to locate the most likely orientations to trace fibers through crossings and bifurcations. In the experiments, we obtain visually correct and promising results. Our future work includes extending the approach to 3-D data, reducing the number of parameters that need to be tuned as well as extending the proposed framework with diffusion tensor data.

7. REFERENCES

[1] D. Rohmer, A. Sitek, and G. T. Gullberg, "Reconstruction and visualization of fiber and laminar structure in the normal human heart from ex vivo DTMRI data," Tech. Rep., Lawrence Berkeley National Laboratory, December 2006.

[2] A. F. Frangi, W. J. Niessen, K. L. Vincken, and M. A. Viergever, "Multiscale vessel enhancement filtering," in *MICCAI*, 1998.

[3] W. J. Karlon, P. P. Hsu, S. Li, S. Chien, A. D. McCulloch, and J. H. Omens, "Measurement of orientation and distribution of cellular alignment and cytoskeletal organization," *Annals of Biomedical Engineering*, vol. 27, pp. 712–720, 1999.

[4] K. Krissian, G. Malandain, N. Ayache, R. Vaillant, and Y. Trousset, "Model based detection of tubular structures in 3D images," *Computer Vision Image Understanding*, pp. 130–171, 2000.

[5] C. G. Harris and M. J. Stevens, "A combined corner and edge detector," in *4th Alley Vision Conf.*, 1988.

[6] T. Aach, C. Mata, I. Stuke, and E. Barth, "Analysis of superimposed oriented patterns," *IEEE Trans. on Image Processing*, vol. 15, no. 12, pp. 3690–3700, December 2006.

[7] M.E. Sargın, A. Altınok, K. Rose, and B. S. Manjunath, "Tracing curvilinear structures in live cell images," in *IEEE Int. Conf. on Image Processing*, 2007, vol. 6, pp. 285–288.

[8] M. Galun, R. Basri, and A. Brandt, "Multiscale edge detection and fiber enhancement using differences of oriented means," in *IEEE Int. Conf. on Computer Vision*, 2007.

[9] X. Qian, M. P. Brennan, D. P. Dione, W. L. Dobrucki, M. P. Jackowski, C. K. Breuer, A. J. Sinusas, and X. Papademetris, "Detection of complex vascular structures using polar neighborhood intensity profile," in *IEEE Int. Conf. on Computer Vision*, 2007.

[10] D. Geman and B. Jedynak, "An active testing model for tracking roads in satellite images," *IEEE Trans. on Pattern Analysis and Machine Intelligence*, vol. 18, pp. 1–14, January 1996.

[11] K.J. Böhm, "Microtubules gliding across kinesin-coated glass surface," http://www.fli-leibniz.de/~kboehm/Kinesin.html.

[12] B. Obara, "Microtubule image," http://boguslawobara.net.